PERGAMON

Control Engineering Practice 10 (2002) 197–206

CONTROL ENGINEERING PRACTICE

www.elsevier.com/locate/conengprac

Modeling and cycling control of carbonate fuel cell power plants ☆

Michael D. Lukas[a], Kwang Y. Lee[a,*], Hossein Ghezel-Ayagh[b]

[a] *Department of Electrical Engineering, The Pennsylvania State University, University Park, PA 16802, USA*
[b] *FuelCell Energy, Inc., Three Great Pasture Rd., Danbury, CT 06813, USA*

Received 20 September 2000; accepted 30 April 2001

Abstract

A mathematical process model for an internal reforming molten carbonate fuel cell power plant is discussed in this paper. The dominant thermal and chemical dynamic processes are modeled for the cell stack array and balance-of-plant, including cathode gas preparation, heat recovery, and fuel processing. Physical data is obtained from a 2 MW system design that was a precursor to a demonstration plant operated at the City of Santa Clara, CA, USA. Steady state validation for several load points is provided for the cell stack array and a load cycling control system is described and tested under ramping operation between load points.

Keywords: Control; Dynamics; Fuel cell plant; Mathematical models; Power generation; Simulation

1. Introduction

Fuel cell-based power plants convert the chemical energy in a fuel directly to electricity without the requirement of conversion of energy into heat. This results in high efficiency (50–60% before heat recovery). In addition, NO_x and SO_x emissions are greatly reduced in comparison with fossil fuel-based generation. Among various types of fuel cell technologies, phosphoric acid fuel cell systems are readily available in 250 kW size. The more efficient next generation molten carbonate fuel cell (MCFC) system has just reached commercial status, with ongoing field β-testing of 250 kW natural gas units. Evolution of the MCFC power plant from research and development to a mature product has commenced with the demonstration of MW-class power plant operation. One of the largest of these demonstrations has been California's 2 MW Santa Clara Demonstration Project (SCDP) (Monn, 1995; Skok, Abueg, Shwartz, & Brodie, 1996). The SCDP is designed using sixteen 125 kW *stacks* of fuel cells that are based on "direct fuel cell technology" developed by FuelCell energy (FCE). This type of fuel cell utilizes internal reforming of natural gas, eliminating the need for a large external reformer to produce hydrogen fuel, simplifying the plant configuration.

Mathematical modeling of fuel cells has concentrated on such issues as physical and transport properties, kinetics, and static performance. Simple, dynamic representations of fuel cells and balance-of-plant (BOP) are instead preferred for use in control applications. To this end, there have been several reported developments in the literature based on particular assumptions. Cell geometry effects and complex mass distributions have been included in a dynamic model for external reforming MCFC (He, 1994, 1995). Alternatively, a dynamic model for internal reforming MCFC has been developed assuming chemical reactions at equilibrium and negligible mass storage (Ernest, Ghezel-Ayagh, & Kush, 1996). The lumped-parameter model outlined in this paper is based on representation of both fast and slow dynamics by considering reforming reaction kinetics, mass storage, and cell polarization losses (Lukas, Lee, & Ghezel-Ayagh, 1999).

Demonstration of the SCDP had focused on certain project criteria: power quality, VAR compensation, NO_x and SO_x emissions, efficiency, runtime hours, availability, reliability, and BOP performance. Ramping operation was somewhat conservative, though, being restricted to at most 4%/min and under the assistance of

☆ An early and shorter version of this paper by the authors, entitled "Modeling, Simulation and control of direct reforming molten carbonate fuel cell power plant" was presented at *2000 IFAC Symposium on Power Plants and Power System Control* in Brussels, Belgium, April 2000.

*Corresponding author. Tel.: +1-814-865-2621; fax: +1-814-865-7065.

E-mail address: kwanglee@psu.edu (K.Y. Lee).

0967-0661/02/$ - see front matter
PII: S0967-0661(01)00110-1

an operator (Fuel Cell Engineering Corporation, 1997). In this paper, a load cycling controller for the SCDP is described and demonstrated for ramping operation of 15%/min between load points over the upper power region.

2. Molten carbonate fuel cell

In FCE's technology, natural gas is internally reformed to hydrogen, partially in an internal reforming unit and partially at the cells. The two-step approach, shown in Fig. 1, is a combination of indirect internal reforming (IIR) and direct internal reforming (DIR) which provides for better thermal management (Farooque, 1993). In the IIR step, a reforming unit (RU) is placed between every 10 fuel cells in the stack, converting about 50% of natural gas to hydrogen prior to entry into the cell anode. Further reforming occurs in the cell anodes (DIR step), which are also loaded with reforming catalysts.

As a result of steam reforming, H_2 is introduced at the porous anode electrode. Oxidant (a mixture of O_2 and CO_2) is introduced at the porous cathode electrode. At the cathode electrode, the oxygen and carbon dioxide in the oxidant stream undergo a reaction to form carbonate ions CO_3^{2-}:

$$\tfrac{1}{2}O_2+CO_2+2e^- \overset{\text{Cathode}}{\rightarrow} CO_3^{2-}. \quad (1)$$

The carbonate ions then migrate to the anode electrode through the molten salt electrolyte. The H_2 is reacted with carbonate ions producing H_2O and CO_2:

$$H_2+CO_3^{=} \overset{\text{Anode}}{\rightarrow} H_2O + CO_2+2e^-. \quad (2)$$

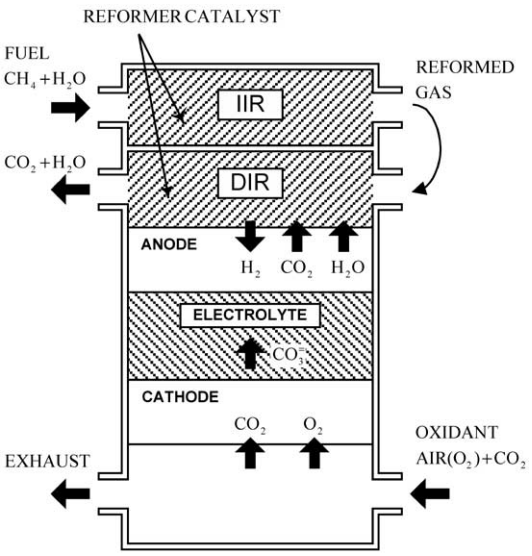

Fig. 1. IIR/DIR structure of MCFC stack.

The following additional, independent reactions occur in both the IIR and the DIR step:

$$CH_4+H_2O \rightarrow CO + 3H_2 \quad \text{Reforming}, \quad (3)$$

$$CO + H_2O \leftrightarrow CO_2+H_2 \quad \text{WGS}, \quad (4)$$

where WGS refers to the water–gas shift reaction. Actual performance (voltage and power) of the fuel cell for a specified load current is determined by the chemical reactants and products as well as cell temperature.

2.1. Stack dynamics

Since each stack in principle operates under the same conditions, the dynamic model considers a lumped representation of all 16 stacks (equivalent stack). Furthermore, the RU and anode compartments are lumped together—subsequently referred to as the *anode*. The model therefore assumes two well-stirred compartments, for each of anode and cathode, with interchange of mass (ions) through the electrolyte matrix separating the two sides. A common stack temperature is assumed and supported by the observation that anode and cathode temperatures are nearly equal. Each anode and cathode compartment has a set of mole balances (Lukas et al., 1999)

$$V\tilde{C}_t\frac{dx_i}{dt} = N^{in}(x_i^{in} - x_i) - x_i\sum_{i=1}^{\xi} R_i + R_i, \quad i = 1, \ldots, \xi, \quad (5)$$

where V is the compartment volume (m^3), $\tilde{C}_t$ the total molar concentration (mol/m^3), N^{in} the total molar flow into volume V (mol/s), x_i^{in} the inlet mole fraction[1] of gas species i, x_i the mole fraction of gas species i, R_i the total production rate of species i (mol/s), and ξ the number of different gas species.

The term R_i represents rate of production of species i due to chemical reaction and can be represented by

$$R_i = \sum_{j=1}^{\mu} v_{ij}r_j, \quad (6)$$

where for a total of μ independent reactions, v_{ij} are the stoichiometric coefficients[2] of species i in reaction j, and r_j the rate of reaction j. Exit stream concentrations in the mole balance equations are replaced by pressures for both the anode and cathode compartments using the ideal gas law $\tilde{C}_t = P/(RT^s)$, where P ($kg/m\,s^2$) is the total gas pressure and R (J/mol K) the universal gas constant. Anode/cathode pressure dynamics (Lukas, Lee, & Ghezel-Ayagh, 2000) are obtained from the ideal gas law by differentiation with respect to time.

[1] Mole fraction is defined as the ratio of moles of gas species i to total moles.

[2] For example, H_2 has a coefficient of 3 in reaction (3).

Assuming that energy accumulates only in the large metal mass, gas mixtures are ideal, and exit stream temperatures are equal to the solid stack temperature, an energy conservation is (Lukas et al., 1999)

$$M^s C_p^s \frac{\mathrm{d}T^s}{\mathrm{d}t} = N_a^{in}\left[\sum_{i=1}^{\xi} x_{ai}^{in}(\bar{h}_{ai}^{in} - \bar{h}_i^s)\right] - \sum_{i=1}^{\xi} \bar{h}_i^s R_{ai} + N_c^{in}\left[\sum_{i=1}^{\xi} x_{ci}^{in}(\bar{h}_{ci}^{in} - \bar{h}_i^s)\right] - \sum_{i=1}^{\xi} \bar{h}_i^s R_{ci} - Q_l - P_{dc}, \quad (7)$$

where subscripts a and c refer to anode and cathode, respectively, and M^s the stack solid mass (kg), C_p^s the stack solid specific heat (J/kg K), T^s the stack solid temperature (K), $\bar{h}_i^{in}$ the inlet molar enthalpy of species i (J/mol), $\bar{h}_i^s$ the molar enthalpy at stack temperature, Q_l the heat loss (W), and P_{dc} the DC electrical power (W).

Ideal gas molar enthalpies for individual species are given by

$$\bar{h}_i = \bar{h}_i^{ref} + \int_{T_{ref}}^{T} c_{p,i}(u)\,\mathrm{d}u, \quad (8)$$

where the first term represents energy at standard reference temperature. Molar heat capacities $c_{p,i}$ (J/mol K) are polynomial functions of absolute temperature, obtained from standard tables. To account for energy changes that occur during chemical reaction, standard heats of formation are included within the reference terms. An important characteristic of Eq. (7) is that the large mass-specific heat (contributed from 16 stacks) results in a thermal time constant of about 6 h.

There are three major reactions in the MCFC: the combined fuel cell reactions (1) and (2); the reforming reaction (3); and the WGS reaction (4). As in Eq. (6), the rate of reaction (j) will be denoted r_j. The overall fuel cell reaction rate for the equivalent stack is determined by Faraday's law of electrolysis (Appleby & Foulkes, 1989)

$$r_1 = r_2 = \frac{-A_r n_{cell} n_{stack} i}{2F} \quad (\mathrm{mol/s}), \quad (9)$$

where i is the fuel cell current density (A/cm^2), n_{cell} the number of cells in stack, n_{stack} the number of stacks, A_r the fuel cell active area (cm^2), and F the Faraday's constant (J/mol V).

In practice, the WGS reaction rapidly approaches near-equilibrium conditions (Xu & Froment, 1989). A quasistatic, equilibrium relationship is therefore used to describe the WGS reaction

$$\frac{x_{CO_2} x_{H_2}}{x_{CO} x_{H_2O}} = \exp(E_1 + E_2/T^s), \quad (10)$$

where E_1 and E_2 are the *Gibb's free energy* constants (Sandler, 1989) for the WGS reaction. Reforming reaction kinetics is commonly defined in terms of

$$CH_4 + 2H_2O \rightarrow CO_2 + 4H_2 \quad (3')$$

which, along with the WGS reaction (4), describes an independent set of reactions equivalent to the set of reactions (3) and (4). The reaction rate of (3′) is (Wolf & Wilemski, 1983)

$$r_{3'} = kP_{CH_4}[(1 - Q)/K_{Meq}] \quad (\mathrm{mol/s}), \quad (11)$$

where k is the reforming rate constant (mol/s), P_{CH_4} the methane partial pressure, Q the mass action expression, and K_{Meq} the reforming reaction equilibrium constant.

Mass action Q is a function of the partial pressures[3] of components in Eq. (5) and the equilibrium constant is $K_{Meq} = \exp(E_3 + E_4/T^s)$, where E_3 and E_4 are the free energy constants for reforming reaction.

Knowledge of the WGS reaction rate r_4 is required in order to evaluate R_i; however, this rate is undefined according to the quasistatic assumption imposed on the WGS reaction. The variable r_4 can be eliminated, though, resulting in an explicit set of equations (Lukas et al., 2000).

2.2. Cell voltage representation

Electrical performance of the fuel cell in terms of temperature and gas compositions is given by the Nernst equation (Hirschenhofer, Stauffer, Engleman, & Klett, 1998)

$$V_0 = E_0(T) + \frac{RT}{2F} \ln \frac{P_{H_2,a} P_{O_2,c}^{1/2} P_{CO_2,c}}{P_{H_2O,a} P_{CO_2,a}}, \quad (12)$$

where V_0 is the equilibrium cell potential (V), $E_0(T)$ the cell standard potential (V), and P_i the partial pressure of gas species i.

Fuel cell irreversible losses are contributed by activation, concentration, and ohmic polarizations:

$$V_{cell} = V_0 - \eta_{act} - \eta_{conc} - iz, \quad (13)$$

where V_{cell} is the cell voltage under load (V), η_{act} the activation polarization (V), η_{conc} the concentration polarization (V), and z the cell ohmic impedance ($\Omega\,\mathrm{cm}^2$).

Polarization losses are generally dependent on gas partial pressures, temperature, and current density, all of which are spatially distributed in an actual cell. Empirical relationships, correlated with cell average quantities, are used to describe polarization losses and cell standard potential. These are obtained from a three-dimensional fuel cell performance model validated with the experimental data (Ding, Patel, Farooque, & Maru, 1997).

[3] Partial pressure $P_i \equiv x_i P/P_{atm}$; P_{atm} is atmospheric pressure.

2.3. Stack model experimental results

Parameters used in the dynamic model include: anode/cathode volumes, stack solid mass and specific heat, cell active area, and reforming catalyst area. Standard constants are used for the WGS and reforming reactions. All parameters represent a 16-stack equivalent, corresponding to the SCDP. The SCDP uses 16 125 kW fuel cell stacks, each consisting of 258 cells. A series connection of four stacks forms a *string* and the system DC voltage is taken across a parallel combination of four strings ($V_{sys} = 4\times258\times V_{cell}$). Table 1 gives a steady state comparison of model and actual plant data (Fuel Cell Engineering Corporation, 1997).

Table 1
Steady state model validation

	System current (A)	System voltage (V)	
		Plant	Model
Full power	3056	750	720
Rated power	2483	791	777
Part load	2101	816	812

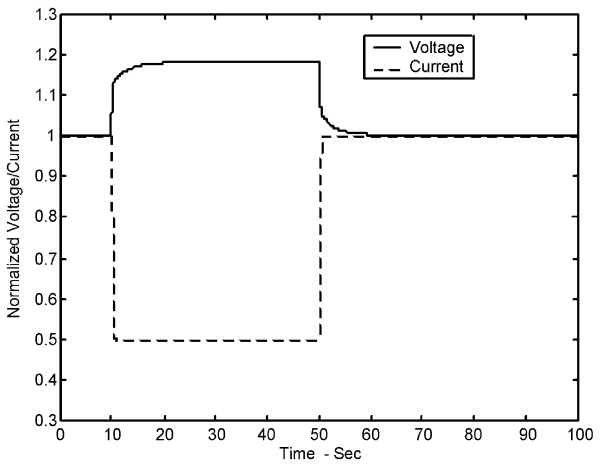

Fig. 2. System voltage response to sudden reduction and restoration of system current.

Fast transient responses are investigated by suddenly removing, and then restoring, 50% of the rated load current while anode/cathode inlet conditions are held constant. Fig. 2 shows the system voltage (normalized to rated value) for this transient. The shape of the voltage profile is in excellent agreement with test data from an MCFC laboratory unit subjected to a similar disturbance (Sasaki, Matsumoto, Tanaka, & Ohtsuki, 1988).

3. MCFC power plant

A simplified process flow diagram for the SCDP is shown in Fig. 3. Major systems include:

1. fuel cell stack array,
2. cathode gas preparation (anode exhaust oxidizer and booster blower),
3. heat recovery (steam and fuel preheating),
4. fuel processing (preconverter and hydrodesulfurizer).

3.1. Cathode gas preparation

The cathode gas preparation system includes the catalytic anode exhaust oxidizer and variable speed-driven booster blower. At the stack cathode, O_2 is supplied by air and CO_2 is made available by recycling the CO_2 from the anode compartment. A small percentage of additional CO_2 is contributed by oxidation of CO (also present at the anode) within the oxidizer. The reactions taking place within the oxidizer are

$$H_2 + \tfrac{1}{2}O_2 \rightarrow H_2O, \tag{14}$$

$$CO + \tfrac{1}{2}O_2 \rightarrow CO_2, \tag{15}$$

$$CH_4 + 2O_2 \rightarrow CO_2 + 2H_2O. \tag{16}$$

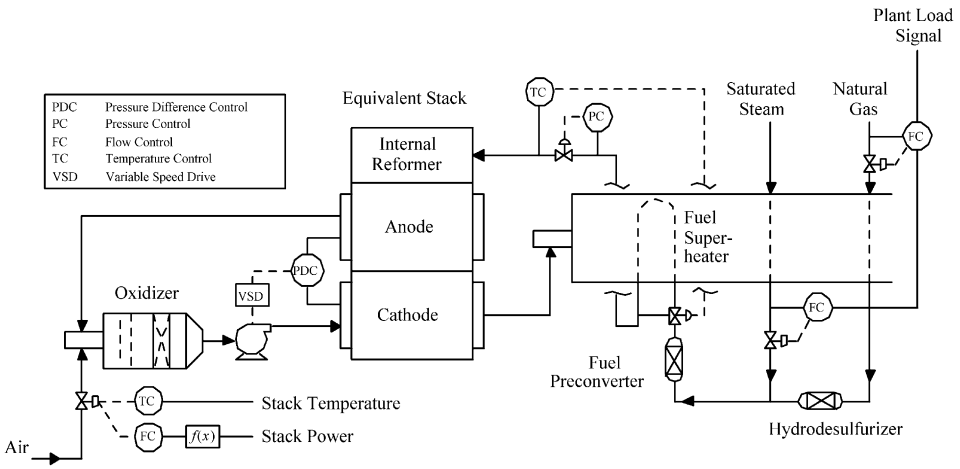

Fig. 3. Simplified process flow diagram for the SCDP.

Reaction (16) occurs primarily during startup operation when supplementary CH_4 is burnt to maintain system temperature. The oxidation reactions are modeled as complete and spontaneous and minimum theoretical air (MTA) required for completion is always available under all plant operating conditions. A set of mole balances, analogous to those in the stack, is applied to the resident gases within the oxidizer: CO_2, H_2O, N_2, and O_2. Energy storage in the oxidizer is also similar to the stack in that there is a significant solid component in the combined catalyst bed and static mixer. Therefore, a similar form for energy conservation is applied, with appropriate modifications to the right-hand side of Eq. (7). Air flow (supplied by a compressor) into the oxidizer is used for stack temperature control and is about seven times larger (on a mass basis) than the MTA required for complete oxidation.

A variable speed-driven blower is used to control differential pressure between anode and cathode. The blower model is described by a polynomial (using identified coefficients from performance data) relating static pressure at rated speed SP_R to actual cubic feet per minute at rated speed $ACFM_R$. Performance at off-rated speed is (Cherkasski, 1980)

$$\begin{aligned} ACFM &= K \cdot ACFM_R, \\ SP &= K^2 SP_R, \\ K &= N/N_R, \end{aligned} \tag{17}$$

where N is the actual blower speed in rpm, and N_R the rated blower speed in rpm.

Blower exhaust temperature is calculated from performance curves of blower efficiency and brake horsepower.

3.2. Heat recovery

The fuel cell stack cathode exhaust gas is a mixture of CO_2, H_2O, N_2, and O_2 at a temperature of about 677°C. This exhaust gas enters the heat recovery unit and exchanges heat with the fuel superheater tube-side gas, a mixture composed mainly of CH_4, H_2O, and H_2, which then enters the RU. Following the fuel superheater, in order, are the steam superheater, steam boiler[4] (not shown in Fig. 3), and fuel preheater. Associated with the fuel superheater is a bypass valve to control the temperature of the steam/methane fuel mixture entering the RU. Another valve is placed between the fuel superheater and RU, used for regulating RU *back-pressure*.

Each superheater is a shell-and-tube heat exchanger. The largest of these, the fuel superheater, has tube-side and shell-side gas volumes of about 0.15 and 1.8 m^3, respectively. As a result, mass storage time constants are at most 0.4 s for either side. The time constant for gas energy storage on the shell-side is roughly the same. When considering energy storage within the metal, however, the time constant is about 4.5 min on the tube-side. This implies the following representation for a superheater:

$$\frac{dH_t}{dt} = \frac{Q - w_t(H_t - H_t^{in})}{M_e}, \tag{18}$$

$$H_s = H_s^{in} - Q/w_s, \tag{19}$$

where $H_t(H_s)$ is the tube (shell)-side enthalpy (J/kg), $H_t^{in}(H_s^{in})$ the tube (shell)-side inlet enthalpy (J/kg), $w_t \times (w_s)$ the tube (shell)-side mass flowrate (kg/s), Q the rate of heat input (J/s) and M_e the effective mass (kg).

The effective mass[5] is a representation of lumped metal and tube-side fluid mass (McDonald, Kwatny, & Spare, 1971):

$$M_e = \alpha M_m \frac{C_{pm}}{C_{pt}} + \rho_t V_t, \tag{20}$$

where M_m is the metal mass (kg), α the ratio of metal to fluid temperature, C_{pm} the metal specific heat (J/kg K), C_{pt} the fluid specific heat (J/kg l K), ρ_t the fluid density (kg/m^3), and V_t the fluid volume (m^3).

Defining effective temperature as the average of inlet and exhaust temperature, $T_e = (T + T^{in})/2$, the rate of heat input in Eqs. (18) and (19) is determined by convection heat transfer (Nam, 1986):

$$Q = Z w_s^{Z_n}(T_{se} - T_{te}), \tag{21}$$

where Z is the identified coefficient (J/kg l K), Z_n the identified coefficient, T_{se} the shell-side effective temperature (K), and T_{te} the tube-side effective temperature (K).

Finally, a relationship between specific enthalpy H and molar enthalpy $\bar{h}_i$,

$$H(T) = \sum_{i=1}^{\xi} x_i \bar{h}_i(T) / \sum_{i=1}^{\xi} x_i M_i, \tag{22}$$

is used to calculate inlet enthalpies in Eqs. (18) and (19), where M_i(kg/mol) represents molecular weight of species i. Conversely, Eq. (22) is used to solve for temperature, given H_t or H_s.

3.3. Fuel processing

Referring to the process flow diagram of Fig. 3, the fuel processing consists of both hydrodesulfurizer and fuel preconverter. The hydrodesulfurizer removes odorants and impurities from natural gas to the level required for fuel cell operation. This reactor has minimal effect on temperature and gas composition because it is primarily used to remove trace amounts (parts per million, ppm) of sulfur compounds. Therefore, only a pressure drop is modeled. Desulfurization occurs at a design inlet temperature of about 370°C,

[4] The boiler model description is omitted for brevity.

[5] Evaluated at steady state, nominal plant conditions.

achieved by preheating the methane and using bypass control (not shown in Fig. 3) for temperature regulation. In practice, the reactor also requires at the inlet an additional, small *slipstream* of H_2, generated elsewhere in the plant.

The preconverter removes higher hydrocarbons (e.g., ethane and propane) from natural gas to preclude the formation of carbon from these hydrocarbons within the stack during temperature transients. This is achieved by steam reforming at lower temperature. At the preconverter inlet is a mixture of steam and natural gas and although natural gas temperature is regulated, steam temperature is unregulated and slowly varying. This is due to coupling with slow stack temperature via heat transfer. Relative to slow inlet disturbances, the reforming reaction kinetics is much faster. Temperature dynamics are also fast due to a small catalyst bed. Therefore, both the reforming reaction (3) and WGS reaction (4) are modeled as quasistatic (i.e., at equilibrium) and energy conservation is modeled at steady state:

$$\sum_{i=1}^{\xi} \bar{h}_i^{in} N_i^{in} = \sum_{i=1}^{\xi} \bar{h}_i N_i, \tag{23}$$

where N_i^{in} and N_i are species i inlet and exhaust molar flows, respectively.

4. Simulated plant cycling control

Throughout this section the load demand profile of Fig. 4 is assumed, where net AC power is defined as the total stack DC power minus losses[6] due to inverter inefficiency and blower and air compressor power consumption. The net AC load demand starts from rated net AC (1809 kW), ramps down to part load (1452 kW), then up to full load (2023 kW). The cycling nature of this particular load demand was chosen to simulate rapid load changes that might be encountered, in say, peak-shaving operation.

There are a number of control loops involved in the MCFC power plant. Among these include: (1) RU inlet temperature; (2) natural gas temperature; (3) RU backpressure; (4) boiler (drum water volume, drum pressure); and (5) load tracking. The RU inlet temperature setpoint varies with load while natural gas temperature, RU backpressure, and drum level and pressure are regulated to fixed setpoints. Load tracking is achieved by a combination of power conditioning system (PCS) and PCS controller, where the PCS includes a DC–AC inverter. The following will concentrate on the remaining control loops:

[6] Losses are modeled using steady state correlations obtained from plant data.

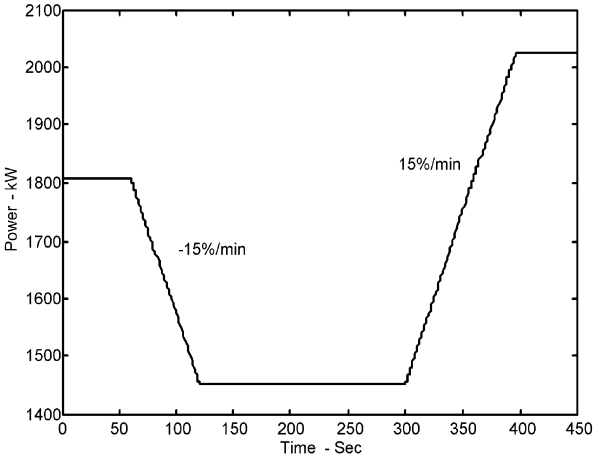

Fig. 4. Net AC load demand profile.

1. fuel utilization,
2. steam–carbon ratio,
3. stack temperature,
4. stack differential pressure.

A complete list of control loops for the SCDP is given in Table 2. All controllers used in the simulation are single-loop, PI-type. In order to observe both fast and slow dynamics of certain controlled quantities, some of the figures in this section employ a logarithmic time scale.

4.1. Fuel utilization and steam–carbon ratio

Fuel utilization is defined as the fraction of total fuel introduced into the cell that reacts electrochemically (Hirschenhofer et al., 1998)

$$U_f \equiv \frac{\mathrm{H}_{2,\,\mathrm{consumed}}}{\mathrm{H}_{2,\,\mathrm{in}}}, \tag{24}$$

where $\mathrm{H}_{2,\,\mathrm{consumed}}$ is the rate of consumption of hydrogen in the electrochemical reaction and $\mathrm{H}_{2,\,\mathrm{in}}$ the molar flowrate of hydrogen into the fuel cell. In the case of an internal reforming MCFC this latter quantity is defined to account for internal generation of hydrogen as well. For the SCDP,

$$\mathrm{H}_{2,\,\mathrm{in}} \equiv N_{ru}^{in}(x_{ru,\,\mathrm{H}_2}^{in} + 4x_{ru,\,\mathrm{CH}_4}^{in} + x_{ru,\,\mathrm{CO}}^{in}), \tag{25}$$

where N_{ru}^{in} is the RU inlet total molar flow and the terms $x_{ru,\,i}^{in}$ represent RU inlet gas mole fractions. Eq. (25) represents H_2 generation from: (1) upstream reaction (preconverter); (2) reforming reaction (RU and cell); and (3) WGS reaction (RU and cell). The coefficients in Eq. (25) follow from reactions (3) and (4). Moreover, Faraday's law (9) can be used to replace $\mathrm{H}_{2,\,\mathrm{consumed}}$ by measurable system DC current I_{sys} (*plant load signal* of Fig. 3) in the expression for fuel utilization. Specific

Table 2
SCDP control loops

Control loop	Controlled quantity	Setpoint	Actuation
1	Stack temperature	676.7°C	Flow valve
2	Stack differential pressure	0.001 bar	Booster blower speed
3	Stack RU back pressure	1.38 bar	Regulator valve
4	RU inlet temperature	Load depend	Bypass valve
5	Steam drum water volume[a]	0.31 m^3	Feedwater flow valve
6	Steam drum pressure[a]	3.45 bar	Pressure relief valve
7	Natural gas temperature[a]	371°C	Bypass valve
8	Natural gas flow	$w^{set}_{nat\ gas}$	Flow valve
9	Steam flow	w^{set}_{steam}	Flow valve
10	Net AC power[a]	Load demand	Inverter current

[a] Not shown in Fig. 3.

application to the SCDP yields

$$U_f = \frac{4 \cdot 258 I_{sys}}{2FH_{2,\,in}}. \tag{26}$$

Steam–carbon ratio is simply defined as the molar ratio of steam to methane:

$$\text{s/c ratio} \equiv \frac{x_{H_2O}}{x_{CH_4}} = \frac{N_{H_2O}}{N_{CH_4}}. \tag{27}$$

Two control objectives under load cycling are:

1. 75% fuel utilization in upper load range,
2. RU inlet s/c ratio at least 2.0.

A fuel utilization of 75% is a design compromise between high voltage and efficient use of available hydrogen, while steam–carbon ratio is lower-bounded in practice to avoid the formation of carbon within the stacks. Both fuel utilization and steam–carbon ratio are manipulated by appropriate combination of natural gas and steam flows; however, neither fuel utilization nor steam–carbon ratio is measured online, in practice. Following the above control objectives, setpoints for mass flowrates of natural gas and steam can be derived. These follow from Eqs. (26) and (27), mass conservation, and the relationship between molar flow and mass flow (Lukas, Lee, & Ghezel-Ayagh, 2001):

$$w^{set}_{nat\ gas} = \frac{K \cdot M_{CH_4} M_{pr} I_{sys}/F}{(M_{CH_4} + 2M_{H_2O})(x_{pr,\,H_2} + 4x_{pr,\,CH_4} + x_{pr,\,CO})}, \tag{28}$$

$$w^{set}_{steam} = \frac{2M_{H_2O}}{M_{CH_4}} w^{meas}_{nat\ gas}. \tag{29}$$

In Eqs. (28) and (29), M_{CH_4} and M_{H_2O} are molecular weights of methane and water, respectively, and K a constant. In Eq. (28), M_{pr} is the average molecular weight and $x_{pr,\,i}$ the species mole fractions, all corresponding to preconverter exhaust. These latter quantities are immeasurable online but are replaced in Eq. (28) by constant values, evaluated at nominal plant conditions (Lukas et al., 2001). Consequently, offsets in steam–carbon ratio and fuel utilization are expected over a range of operation. Measurable quantities include system current I_{sys} in Eq. (28) and measured natural gas flow $w^{meas}_{nat\ gas}$ in Eq. (29).

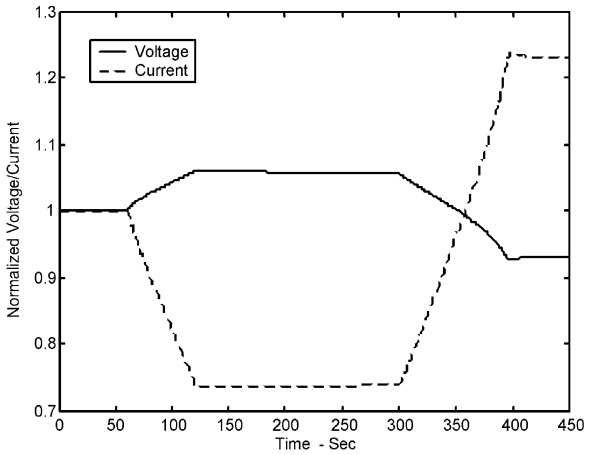

Fig. 5. System current and voltage under load cycling.

Under PCS control, system DC current is adjusted so that net AC power follows the demand power. System DC voltage is unregulated, however. Both of these are shown in Fig. 5, subject to the load cycle of Fig. 4.

As a result of the calculations in Eqs. (28) and (29), natural gas and steam flow setpoints, shown in Fig. 6, take the shape of system current. Fuel utilization and steam–carbon ratio are shown in Figs. 7 and 8, respectively. Both of these are subject to steady state offset as well as increased offset during ramping stages due to the inability of PI controllers in tracking polynomials with zero error. The axes in Fig. 7 are chosen to highlight this effect. Both fuel utilization and steam–carbon ratio depend on immeasurable variables M_{pr} and $x_{pr,\,i}$, which in turn depend on slow temperature. The axes in Fig. 8 are chosen to highlight this slow response. Deviations in both fuel utilization and steam–carbon ratio are very small. This is attributed largely to the ability of both steam and natural gas flows in tracking the rate-limited flow setpoints of Fig. 6, apart

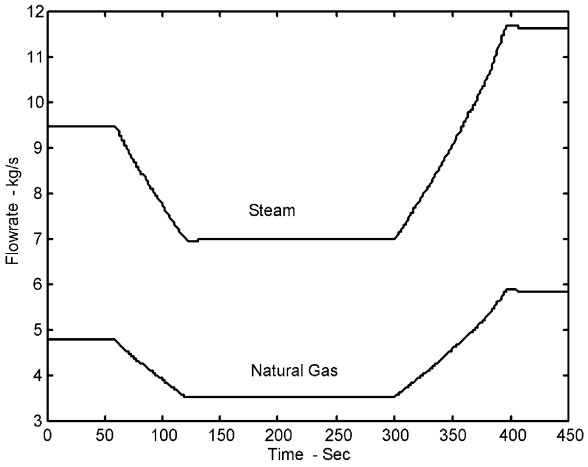

Fig. 6. Natural gas and steam flow setpoints.

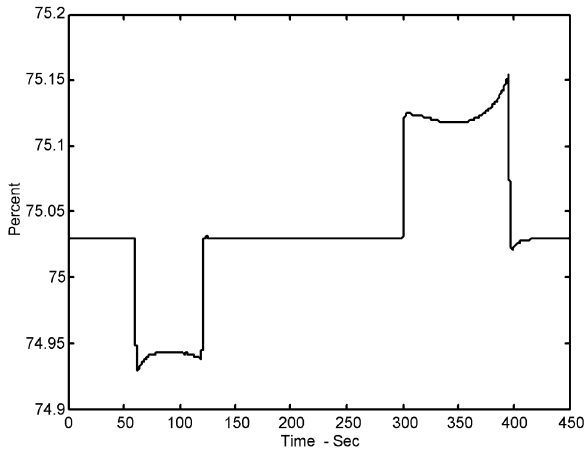

Fig. 7. Fuel utilization.

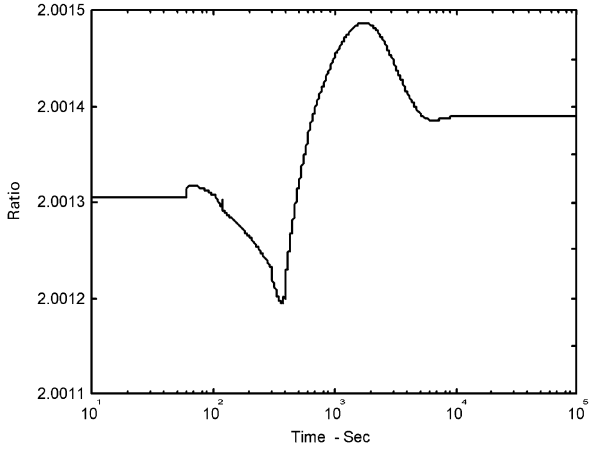

Fig. 8. RU inlet steam–carbon ratio.

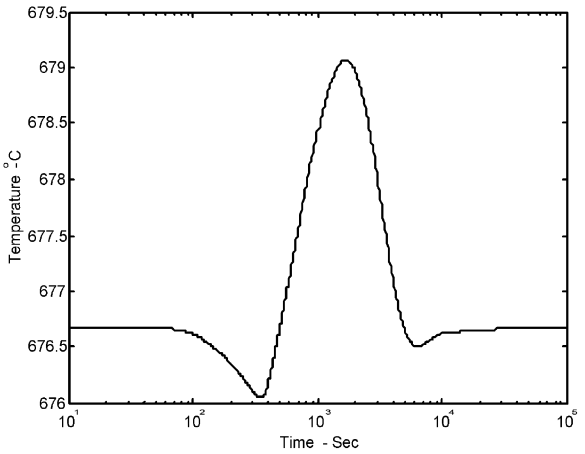

Fig. 9. Stack temperature.

from additional offsets as described above. Under sudden load changes, however, the deviations are potentially much greater (Lukas et al., 2001).

4.2. Stack temperature

Stack temperature is controlled to prevent the formation of carbon within the stack during temperature transients. Control is achieved by adjusting the air flow into the oxidizer. Due to the large (equivalent) stack thermal time constant, feedback alone is not adequate; feedforward control is additionally used. Referring to Fig. 3, this is implemented with an extra flow controller (PI-type) using stack power[7] as the measurable disturbance. The function $f(x)$ is a static mapping relating steady state electrical power and steady state air flow. This provides a flow setpoint corresponding to any measurable stack power. The advantage is that a rapid change in air flow is possible, enabling a much tighter control of stack temperature than with slow feedback alone. Stack temperature, shown in Fig. 9, has a constant setpoint of about 676.7°C and is seen to settle within roughly 3 h. As a result of static feedforward control, oxidizer air flow in Fig. 10 follows the load profile in Fig. 4, initially, until feedback trim control starts taking effect. This occurs when the error between stack temperature and stack temperature setpoint becomes significant as time gets larger.

4.3. Stack differential pressure

Neither anode pressure nor cathode pressure is controlled but differential pressure between anode and cathode is regulated to a fixed setpoint of about 0.001 bar. Peak differential pressure is limited in practice to about 0.035 bar to avoid gas crossover from one compartment to another. Varying the speed of the booster blower controls differential pressure.

Rapid load changes are followed by rapid changes in mass inventory within both stack anode and stack cathode, causing pressure changes in each. There are

[7] Stack power is P_{dc} in Eq. (7).

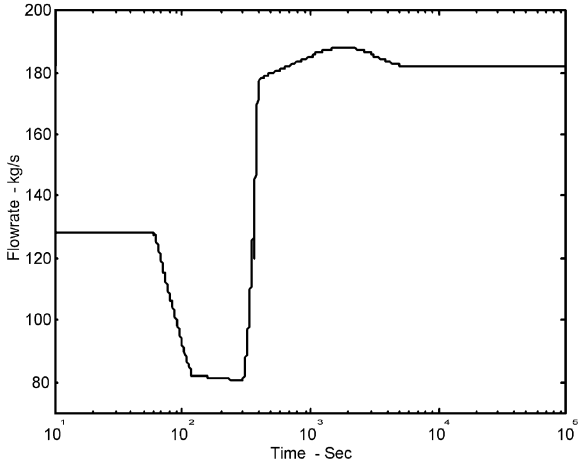

Fig. 10. Oxidizer air flow.

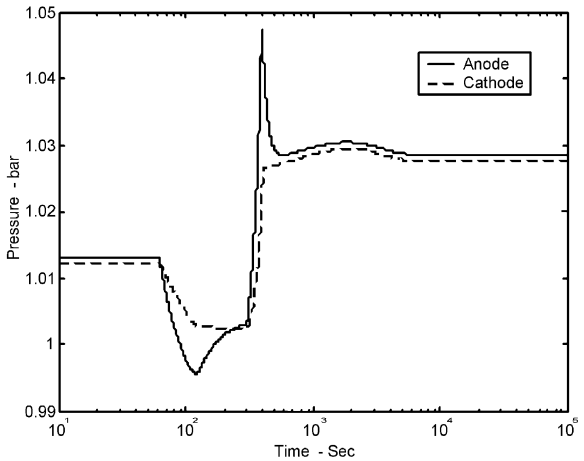

Fig. 11. Anode and cathode pressures.

two main contributions: (1) setpoint changes in steam/methane flows to maintain fuel utilization and steam–carbon ratio, and (2) changes in oxidizer flow resulting from static feedforward control of stack temperature. Anode and cathode pressures, though, each consist of fast dynamics driven by changes in mass inventory and slow dynamics due to coupling with slow stack temperature (Lukas et al., 1999).

Fig. 11 shows stack anode/cathode pressures under differential pressure control, subject to the load cycle of Fig. 4. Although pressure difference deviates considerably from its setpoint the peak deviation is still within its limit. After the initial fast transients, anode and cathode pressures are seen to respond slowly as a result of temperature dependence. Fig. 12 shows booster blower speed.

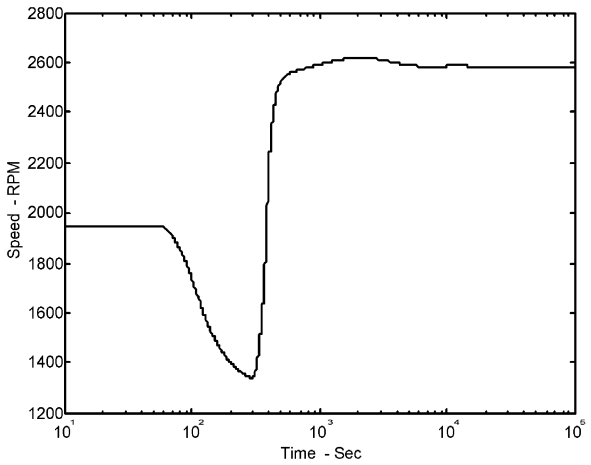

Fig. 12. Booster blower speed.

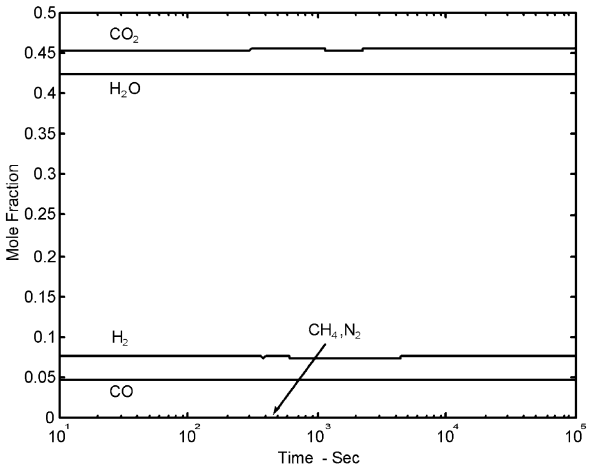

Fig. 13. Anode gas composition.

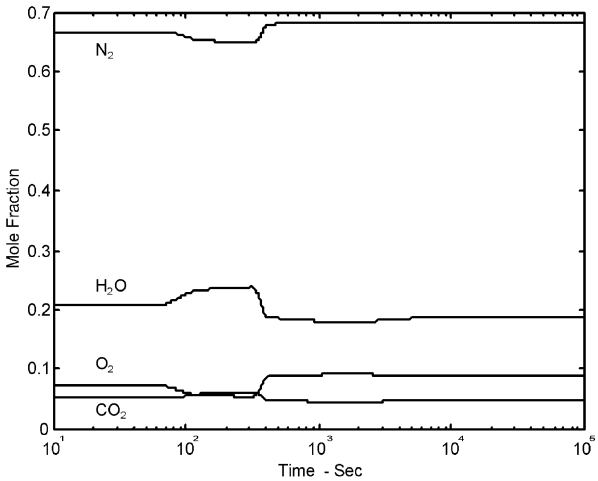

Fig. 14. Cathode gas composition.

4.4. Anode and cathode gas compositions

It is instructive to examine the gas composition of both anode and cathode under cycling control. Anode gas composition is shown in Fig. 13 while Fig. 14 shows cathode gas composition. In the former, gas mole fractions are seen to be nearly invariant—a result of fuel utilization control. Furthermore, methane

conversion to hydrogen is seen to be practically complete[8] as a result of the combined IIR/DIR process. Gas composition at the cathode changes considerably during load cycling and is influenced mainly by changes in oxidizer air flow to maintain stack temperature. Higher loads require proportionally more air flow, causing a shift towards nitrogen and oxygen.

5. Conclusions

The modeling and control aspects of an internal reforming MCFC power plant were described in this paper. Simplifying assumptions led to dynamic models for the equivalent stack and BOP subsystems: cathode gas preparation, heat recovery, and fuel processing. Design data and physical parameters were obtained from a demonstration power plant. A steady state validation for the fuel cell stack array at several load points suggests a reasonable match between model and plant.

The process model is utilized to demonstrate the plant capability of load cycling at a rate of 15%/min, well above typical utility specifications. An initial design for load cycling control, based on single-loop PI controllers, is demonstrated for an important set of control loops: fuel utilization, steam–carbon ratio, stack temperature, and stack differential pressure. Fuel utilization and steam–carbon ratio, additionally, are not measured in practice; this requires proper calculations for flow setpoints.

In this paper, plant operation has been restricted to the upper 30% power range to avoid some complexities of actual plant operation: (1) fuel utilization at lower power is not fixed at 75%, and (2) supplemental burning of natural gas at lower power is necessary to maintain system temperature. Future work points to the inclusion of these features into the process model and controller in order to increase the dynamic range for load cycling. As a result of deeper load cycling the performance objectives are expected to be challenged, and may not be met with the existing control design. Regarding the existing, practical control of fuel utilization and steam–carbon ratio, an enhancement would be the use of a gas composition estimator to avoid the open-loop nature of these control loops.

Acknowledgements

This work is supported by the NSF grant "Intelligent Control and Dynamic Simulation of MCFC Power Plants as Distributed Generation Systems" (DMI-9460694).

[8] Any residual CH_4 is oxidized via (16).

References

Appleby, A. J., & Foulkes, F. R. (1989). *Fuel cell handbook*. New York, USA: Van Nostrand Reinhold.

Cherkasski, V. M. (1980). *Pumps, fans, compressors*. Moscow, RU: Mir Publishers.

Ding, J., Patel, P. S., Farooque, M., & Maru, H. C. (1997). A computer model for direct carbonate fuel cells. *Proceedings of the 4th international symposium on carbonate fuel cell technology*, Montreal, Quebec, CA, (pp. 127–138).

Ernest, J. B., Ghezel-Ayagh, H., & Kush, A. K. (1996). Dynamic simulation of a direct carbonate fuel cell power plant. *Proceedings of the 1996 fuel cell seminar*, Orlando, FL, USA, (pp. 75–78).

Farooque, M., Maru, H. C., & Baker, B. (1993). Direct carbonate fuel cell power plant design at ERC. *Proceedings of the 28th intersociety energy conversion engineering conference*, Atlanta, GA, USA, (pp. 1181–1193).

Fuel Cell Engineering Corporation (1997). Santa Clara 2-MW fuel cell demonstration power plant test report, prepared for EPRI, TR-108252, USA.

He, W. (1994). A dynamic performance of a molten carbonate fuel cell in power generation system. *Journal of Power Sources*, *52*, 179–184.

He, W. (1995). Three-dimensional simulation of a molten carbonate fuel cell stack using computational fluid dynamic techniques. *Journal of Power Sources*, *55*, 25–32.

Hirschenhofer, J. H., Stauffer, D. B., Engleman, R. R., & Klett, M. G. (1998). *Fuel cell handbook*. US, Department of Energy.

Lukas, M. D., Lee, K. Y., & Ghezel-Ayagh, H. (1999). Development of a stack simulation model for control study on direct reforming molten carbonate fuel cell power plant. *IEEE Transactions on Energy Conversion*, *14*(4), 1651–1657.

Lukas, M. D., Lee, K. Y., & Ghezel-Ayagh, H. (2000). Reduced-order dynamic model of carbonate fuel cell system for distributed generation control. *Proceedings of the 2000 IEEE power engineering society summer meeting*, Seattle, WA, USA (pp. 1793–1797).

Lukas, M. D., Lee K. Y., & Ghezel-Ayagh, H. (2001). Performance implications of rapid load changes in carbonate fuel cell systems. *Proceedings of the 2001 IEEE power engineering society winter meeting*, Columbus, OH, USA (pp. 979–984).

McDonald, J. P., Kwatny, H. G., & Spare, J. H. (1971). A nonlinear model for reheat boiler-turbine-generator systems; part II-development. *Proceedings of the joint automatic control conference*, St. Louis, MO, USA, (pp. 227–236).

Monn, M. (1995). Project brings fuel cell closer to utility use. *Power*, *139*(4), 76–79.

Nam, H. (1986). Modeling and control system design of a coal fired power plant. Ph.D. dissertation, University of Texas, Austin, USA.

Sandler, S. I. (1989). *Chemical and engineering thermodynamics*. New York, USA: Wiley.

Sasaki, A., Matsumoto, S., Tanaka, T., & Ohtsuki, J. (1988). Dynamic characteristics of a molten carbonate fuel cell stack. *Proceedings of the IEEE conference on decision and control* (pp. 1044–1049). Austin, TX, USA.

Skok, A. J., Abueg, R. Z., Shwartz, P. H., & Brodie, M. N. (1996). Power conversion and quality of the Santa Clara 2 MW direct carbonate fuel cell demonstration plant. *Proceedings of the 1996 fuel cell seminar* (pp. 83–86) Orlando, FL, USA.

Wolf, T. L., & Wilemski, G. (1983). Molten carbonate fuel cell performance model. *Journal of the Electrochemical Society*, *130*(48), 48–55.

Xu, J., & Froment, G. (1989). Methane steam reforming: II. Diffusional limitations and reactor simulation. *AIChE Journal*, *35*(1), 97–103.